THE JOURNAL OF PHYSICAL CHEMISTRY C

Article

pubs.acs.org/JPCC

Influence of Sn and Cr Doping on Morphology and Luminescence of Thermally Grown Ga_2O_3 Nanowires

Iñaki López, Emilio Nogales,* Bianchi Méndez, and Javier Piqueras

Departamento de Física de Materiales, Facultad de Ciencias Físicas, Universidad Complutense de Madrid, 28040 Madrid, Spain

Andrea Peche, Julio Ramírez-Castellanos, and Jose M. González-Calbet

Departamento de Química Inorgánica, Facultad de Ciencias Químicas, Universidad Complutense de Madrid, 28040 Madrid, Spain

ABSTRACT: Elongated micro- and nanostructures of Sn doped or Sn and Cr codoped monoclinic gallium oxide have been grown by a thermal method. The presence of Sn during growth has been shown to strongly influence the morphology of the resulting structures, including Sn doped branched wires, whips, and needles. Subsequent codoping with Cr is achieved through thermal diffusion for photonic purposes. The formation mechanism of the branched structures has been studied by transmission electron microscopy (TEM). Epitaxial growth has been demonstrated in some cases, revealed by a very high quality interface between the central rod and the branches of the structures, while in other cases, formation of extended defects such as twins has been observed in the interface region. The influence of dopants on the energy levels of Ga and O within the structures has been studied by XPS. Micro-Raman spectroscopy was used to assess the influence of Sn doping, and Sn−Cr codoping, on the vibrational properties of single nanowires. Cathodoluminescence (CL) measurements show a Sn-related complex band in the Sn-doped structures. Temperature-dependent and excitation-density-dependent CL indicates that this is a thermally activated emission. In the Sn−Cr codoped samples, the characteristic, very intense Cr^{3+} red luminescence emission quenches the bands observed in the Sn-doped samples. Branched, Sn−Cr codoped structures were studied with microphotoluminescence imaging and spectroscopy, and waveguiding behavior was observed along the trunks and branches of these structures.

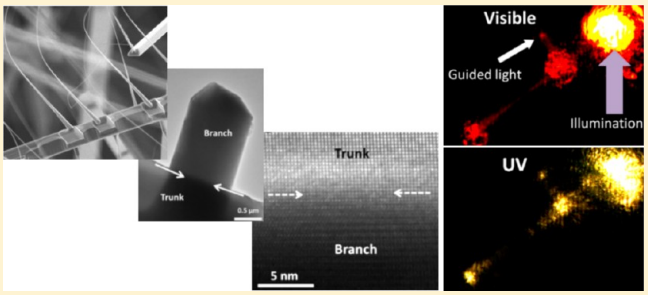

1. INTRODUCTION

Monoclinic β-Ga_2O_3 is a transparent conductive oxide (TCO) with high thermal and chemical stability and controllable n-type conductivity with suitable doping. Impurities in semiconductor matrixes are key factors for improving electrical conductivity, supplying mobile carriers or introducing electronic traps in the band gap, which influence not only their electrical but also their optical properties. Besides the tuning of its physical properties, the control of the dimensionality and morphology is also relevant for the applications of semiconductor oxides in areas of nanoscience and nanotechnology.[1,2] This point has been less explored, and the control of the nanostructures morphology by the addition of impurities during the growth process is worth investigating. Gallium oxide nanowires have been proposed for several applications, such as gas sensors,[1] solar blind sensors in the UV range,[3] white light emitting devices,[4] or waveguides for the UV−vis ranges,[5,6] among others. Regarding its electrical and optical properties, Ga_2O_3 behaves as an n-type semiconductor due to the presence of a donor band related to intrinsic defects and/or native impurities[7,8] and is transparent in the blue-UV range. An effective tuning of electrical or optical properties by the addition of impurities in oxide nanowires is still a challenge, because of the out-diffusion processes and, in many cases, of the low diffusivity of the impurities in nanowires.[9] In the past years, enhancement effects of the gas sensitivity, conductivity, or field-emission properties of Ga_2O_3 by Sn doping have been reported.[7,10−12] With regard to optical properties, light emission from tin doped gallium oxide has also been studied, and blue-green luminescence emission bands linked to the Sn dopant were reported.[10,13] In the above-mentioned works, the study of the influence of Sn doping was focused into the detection of changes in the physical properties of doped gallium oxide; however, the nanowire morphology was retained during the growth process. Undoped gallium oxide nanowires have been obtained by several thermal methods with the aid of metal nanoparticles[2] or by catalyst-free methods.[14,15] In order to dope the nanowires, a possible route is starting with an alloy or a mixture of the precursor elements required, as reported for example in refs 5 and 14. We have previously grown undoped Ga_2O_3 nanowires by using pure metal as gallium source and carrying out a controlled thermal treatment under a dynamic atmosphere in an open furnace.[6,14] To get

Received: September 21, 2012
Revised: December 17, 2012
Published: January 4, 2013

   dx.doi.org/10.1021/jp3093989 | J. Phys. Chem. C 2013, 117, 3036−3045

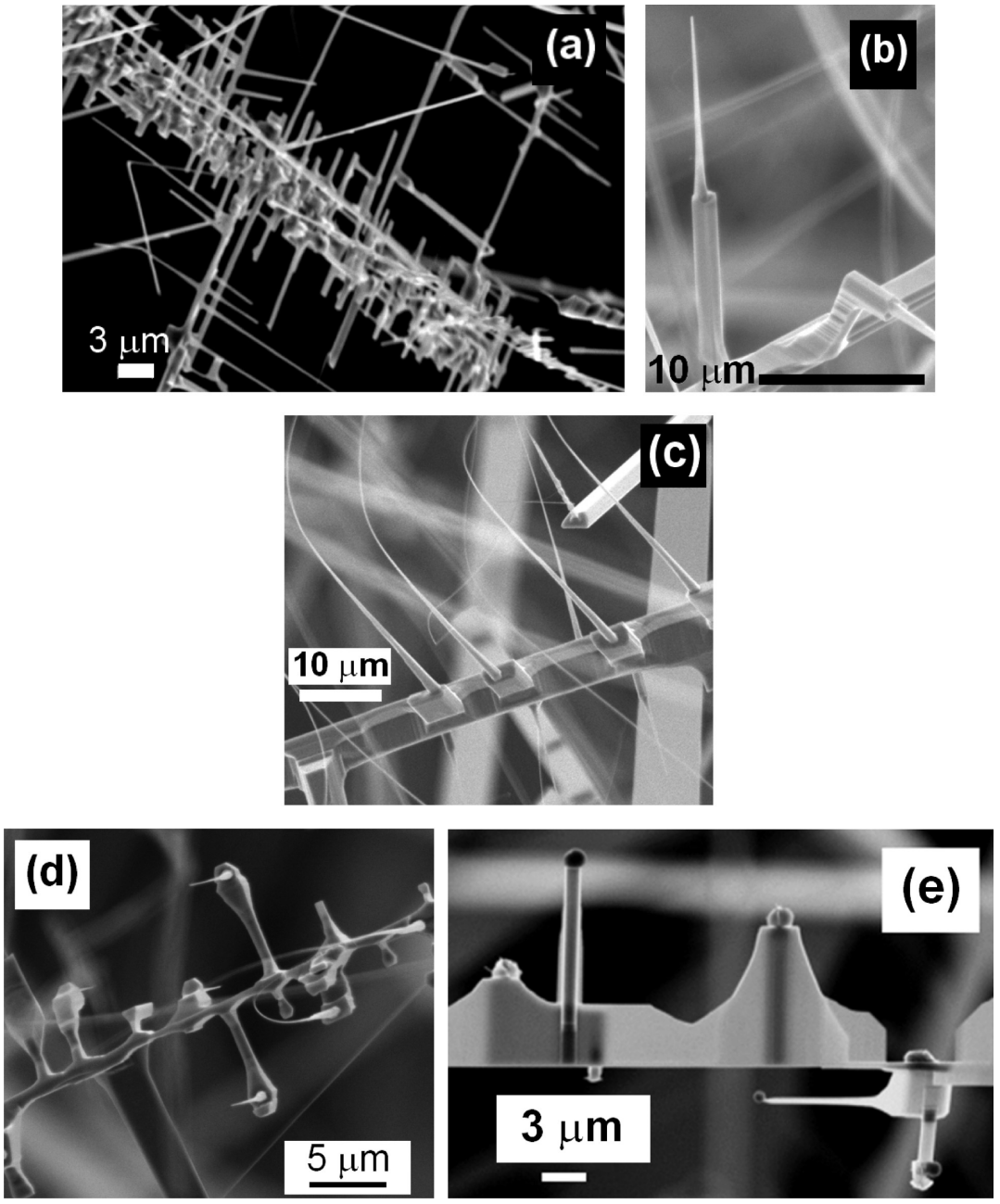

Figure 1. SEM images of Sn doped β-Ga_2O_3 micro- and nanostructures: (a) branched structures, (b) needle structure, (c) whiplike structure, (d) complex needle structures, and (e) branched structures with a round particle at the end of the tip.

doped nanowires within this approach, suitable precursors have to be incorporated into the furnace.[5,14,16]

In this work, SnO_2 or Cr_2O_3 and metallic Ga were used as starting materials, and as a result of the thermal treatment, branched and complex structures with incorporation of dopants were obtained. The results show that Sn impurities may be used to modify the morphology of the resulting nanostructures. The morphological and structural characterization of these branched structures and a tentative explanation of the growth process are provided.

2. EXPERIMENTAL SECTION

The Sn doped β-Ga_2O_3 structures were grown by thermal oxidation at 1100 °C of metallic Ga in the presence of SnO_2 under an inert gas flow on a Ga_2O_3 pellet used as substrate. The same procedure has been reported for undoped Ga_2O_3 nanowires elsewhere.[14] The morphology of the doped structures is influenced by the presence of tin during growth resulting for example in the formation of branched structures, as we will see below. Some of these structures were gently detached from the pellet and placed on a silicon wafer for further characterization. In a second stage, the rest of the structures were used as starting material to obtain codoped (Sn,Cr)-Ga_2O_3 branched structures by a further thermal treatment at 1500 °C for 15 h in the presence of chromium oxide powders. After the growth, the codoped structures were removed from the pellet and placed on a silicon wafer for further characterization.

Morphological characterization has been carried out in a FEI Inspec S50 scanning electron microscope (SEM) and a Leica

dx.doi.org/10.1021/jp3093989 | J. Phys. Chem. C 2013, 117, 3036−3045

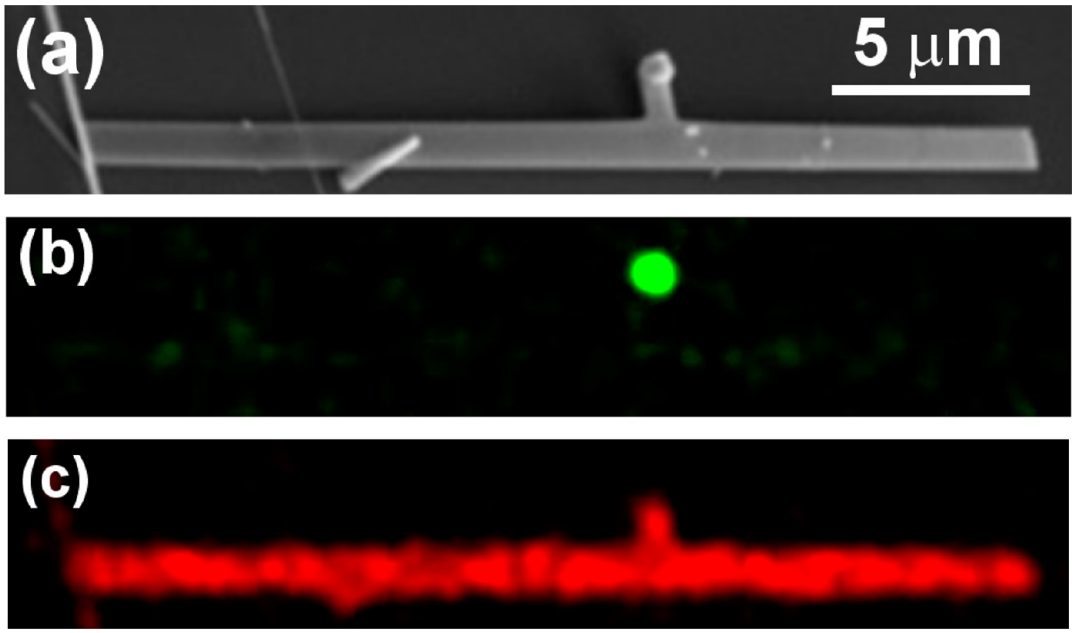

Figure 2. (a) SE image and EDX (b) Sn and (c) Ga maps of a branched structure. The droplet in the end of the branch is shown to be composed by Sn.

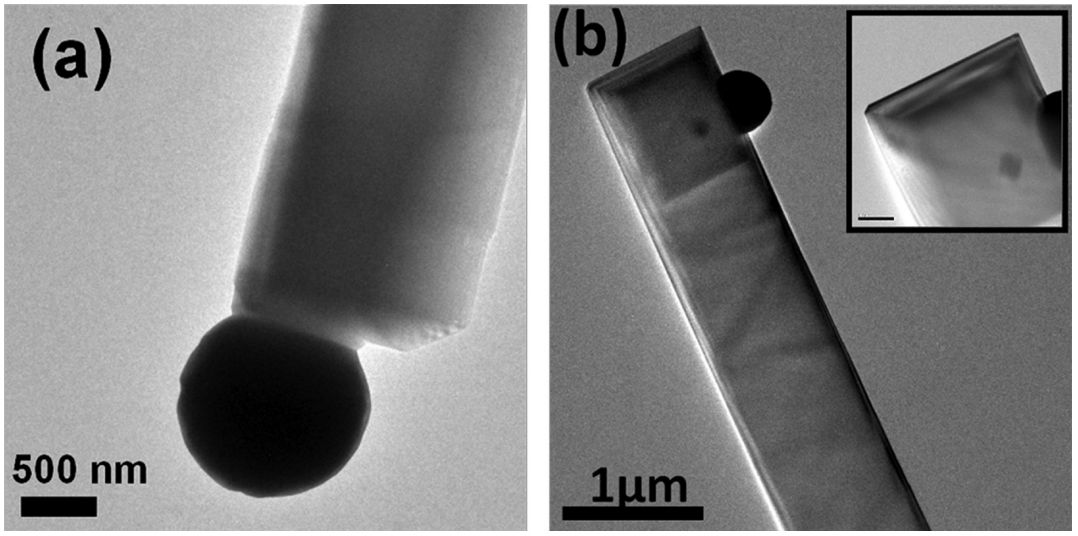

Figure 3. Low magnification bright-field TEM images of Sn doped Ga_2O_3 wires: (a) a nanowire with a Sn ball in its tip and (b) nanoribbon shaped structure. The inset shows the morphological shape of the nanostructure end.

Stereoscan 440 SEM. Selected area electron diffraction (SAED) and high resolution transmission electron microscopy (HRTEM) were performed in a JEOL 3000 FEG electron microscope, fitted with a double tilting goniometry stage (±22°, ± 22°). Simulated HRTEM images were calculated by the multislice method using the MacTempas software package. Energy dispersive X-ray microanalysis spectroscopy (EDS) and cathodoluminescence (CL) measurements were carried out in the above-mentioned Leica SEM. Photoluminescence (PL) spectroscopy and imaging have been performed in a Horiba Jobin Ybon LabRam HR800 Raman confocal microscope. The excitation light was the 325 nm line of a HeCd laser. All PL measurements were performed at room temperature. Raman measurements and XRD were also performed to assess the crystal quality of the wires. The study of the structures was complemented with the aid of high resolution photoemission spectra and imaging, performed at the Sincrotrone Elettra Trieste facility (ESCA microscopy line).

3. RESULTS AND DISCUSSION

3.1. Influence of Doping on Morphology and Crystalline Structure. Figure 1 shows representative SEM images of Sn-doped (Figure 1a–e) Ga_2O_3 structures grown on a gallium oxide compacted pellet. The Sn doped structures present a branched shape (Figure 1a), with trunks whose lengths can reach several hundred micrometers and widths in the range of a few hundred nanometers up to a few micrometers. The branches tend to reach up to several micrometers in length and have widths in the range of a few hundred nanometers. Needlelike (Figure 1b) and whiplike (Figure 1c) structures are also formed in the Sn doped structures obtained by this method. Similar kinds of whiplike

dx.doi.org/10.1021/jp3093989 | J. Phys. Chem. C 2013, 117, 3036–3045

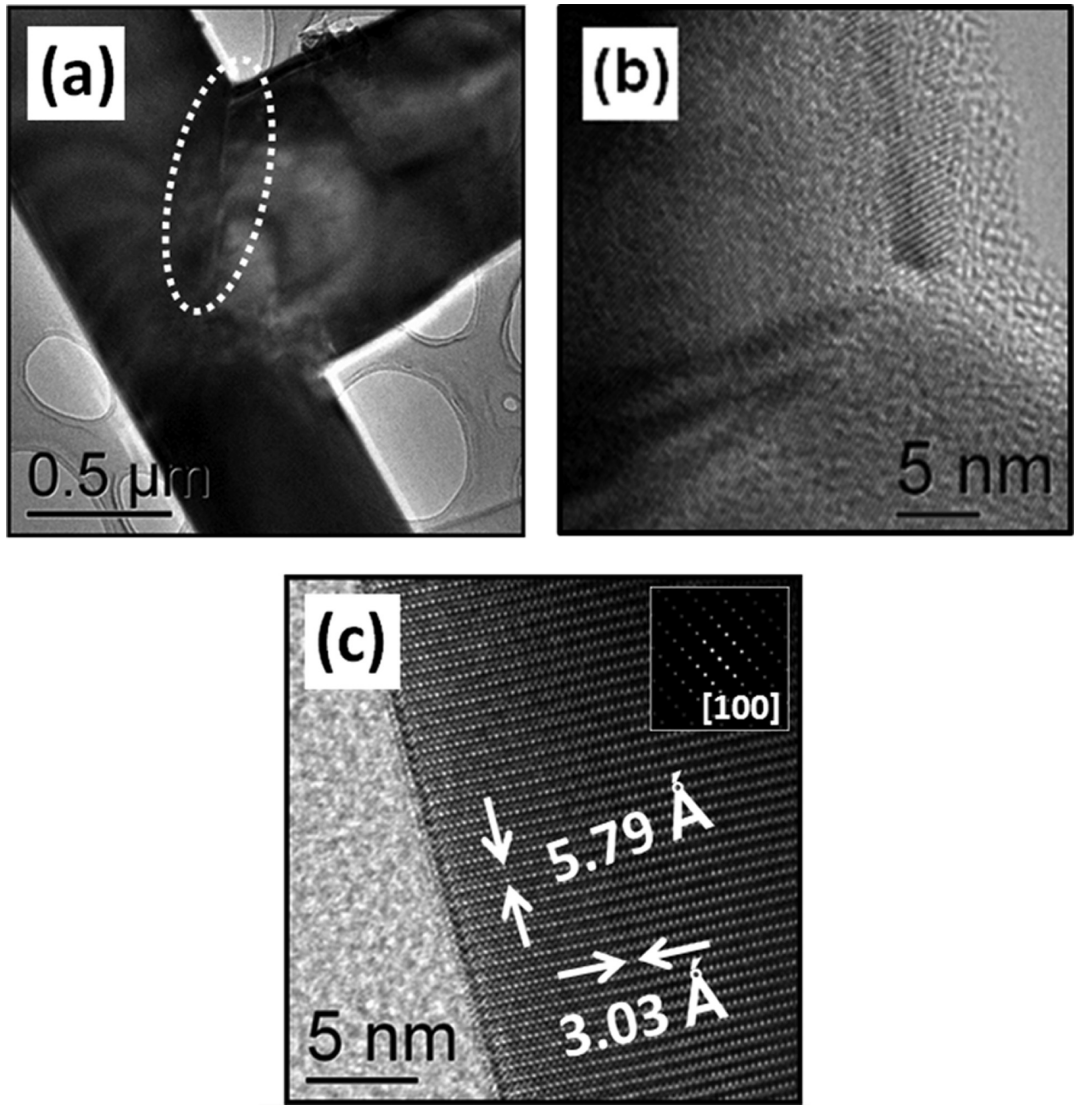

Figure 4. (a) Region where the branch starts growing from the trunk at lower magnification. The dashed ellipse highlights the presence of an extended defect that separates the trunk and the branch. (b) The HRTEM image of the interface and (c) HRTEM image of a branch corresponding to the [100] zone axis shown in the inset.

structures have been also observed in Sn doped GeO_2.[17] XRD measurements (not shown) of Sn doped complex structures show that the crystal structure of the nanowires mesh is the monoclinic β-Ga_2O_3 (JCPDS 00-041-1103). No peaks corresponding to other phases are found. In some cases (Figure 1e), the presence of droplets at the end of a secondary branch is observed. Some of the synthesized structures were placed onto silicon wafer substrates for X-ray microanalysis in the SEM. Figure 2a shows the SEM image of one branched wire with a round particle at the end of its branch. These round particles are also observed in Figure 1e. Figure 2b,c shows the corresponding EDX mapping for Sn and Ga, respectively, showing that the particle at the end of the branch is composed by tin. These observations point out to the formation of small tin aggregates at the surfaces of the primary wires, which favors the catalytic growth of secondary branches. Therefore, as a result of the growth process, the tin droplet could be formed, leaving behind Sn doped β-Ga_2O_3 nanowires. This feature was also observed for Si doped β-Ga_2O_3 nanostructures grown by a similar method.[18]

The small lateral branches of the complex structures were investigated by TEM. Low magnification bright-field TEM images of such structures are depicted in Figure 3. They have nanobelt shape with average lateral size of around 1 μm. Figure 3a shows a nanobelt with a tin ball, which was found to be amorphous, at its end. This shows the existence of a metal-catalyzed vapor−liquid−solid (VLS) growth mechanism.[2] The EDS microanalysis performed within the TEM shows that the chemical composition of this droplet is Sn, in agreement with the results shown in Figure 2 for EDX in the SEM. In the VLS mechanism the metal particle size usually determines the wire diameter, but in our case, the width of the belt does not perfectly fit to the tin ball diameter. On the other hand, tin balls have also been observed attached to the lateral surface of the belts as Figure 3b shows. The inset in Figure 3b shows the detail of the final end of the belt with a flat shape. These results support that tin could play a catalyst-like role in order to develop elongated structures. However, as tin particles are formed not only at the end of the wires, but also at lateral points along the main trunk, branched structures are formed, as observed.

dx.doi.org/10.1021/jp3093989 | J. Phys. Chem. C 2013, 117, 3036−3045

Figure 4 shows the TEM and HRTEM images of a branched structure. The region where a branch starts growing from the trunk is shown in Figure 4a. Figure 4b shows a HRTEM image, with the detail of the defect marked with a dashed line in Figure 4a. Both images show the existence of defects; however, there is structural continuity from the trunk to the branch (Figure 4b). Figure 4c shows a very well-crystallized branch, where the measured interplanar distances of 5.79 Å and 3.03 Å correspond to the [100] zone axis (inset). The growth direction obtained from this image is [001].

These branched structures could be interesting for applications in light generation, detection, or waveguiding.[19] Therefore, it is important to note that the microstructure is crucial in order to understand how light generates or propagates through the nanostructures, since extended defects can be sometimes observed and may act as dispersion centers.

We have studied the possibility of tuning the optical properties of these branched structures by suitable doping with optically active ions, such as Cr, while keeping the branched morphology. Cr ions are chosen because of their high quantum efficiency and the characteristic shape of their red emission bands in gallium oxide nanostructures.[16] To this purpose a thermal treatment of the branched structures in the presence of chromium oxide powders was performed. This subsequent codoping with Cr does not modify essentially the branched morphology of the structures, as shown in Figure 5. However, the structures tend to further grow, and the lateral dimensions were slightly increased.

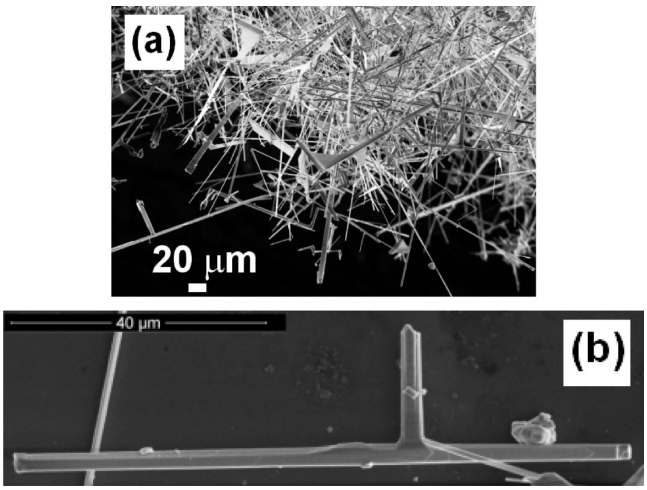

Figure 5. SEM images of codoped Sn, Cr Ga_2O_3 branched wires: (a) structures on the pellet and (b) a single structure on silicon wafer.

In order to characterize the crystal quality of Cr doped branched structures after the Cr diffusion process, some samples were studied by TEM. Figure 6a shows the low magnification TEM image of one of these branched structures, where a junction of a trunk and a branch marked by arrows in the figure, is observed.

The SAED along the [100] zone axis corresponding to the branch is depicted in Figure 6b. The HRTEM image at higher magnification of the same area (Figure 6c) shows a very well-crystallized material. No structural defects are present. The measured interplanar distances are 3.03 and 5.79 Å, which fit well to the b and c parameters of the β-Ga_2O_3 unit cell, respectively, and are the same as those shown in Figure 4c for the Sn doped sample. As in that case, the growth direction obtained from this image is [001]. EDS microanalysis performed on this branch shows a very homogeneous chemical composition and confirms the presence of Sn and Cr.

Figure 7a shows a HRTEM image of a junction area, where two different crystal orientations are observed, that corresponds to the trunk and the branch, respectively. The FFT pattern along [201] (Figure 7b) was obtained from the trunk. Its I-FFT shows a contrast due to heavy atom positions and typical interplanar distances (3.03 and 3.33 Å) of the monoclinic β-Ga_2O_3 phase (Figure 7c). On the other hand, the FFT pattern of the branch is depicted in Figure 7d, which can be indexed along the [100] zone axis. The corresponding I-FFT image (Figure 7e) shows the interplanar distances a = 3.03 and c = 5.79 Å. Finally, the FFT pattern (Figure 7f) of the junction area (marked by dashed arrows in Figure 7a) reveals the overlapping of the diffraction spots of both branch and trunk FFT patterns, which reveals a good match between both crystal orientations. The first layers of the branch seem to adjust quite well, suggesting a good epitaxial growth of these branched structures and a very high crystal quality. It should be noticed that actually, during the Cr diffusion process, no extra tin was incorporated into the furnace, and only chromium oxide powders were added for doping purposes. The Sn doped branched morphology is retained after the doping process, although an overgrowth of the structures is achieved, as we have already shown.

This TEM analysis indicates that epitaxial growth is responsible for the growth of some branches in these samples, as seen in Figures 6 and 7. In other cases, however, the growth of branches is related to the formation of extended defects, such as twins, as observed in Figure 4. In all cases, the branches present very high crystal quality.

3.2. Influence of Doping on Raman Spectra and Chemical Bonds. The local structure of chemical bonds in Sn doped and Sn and Cr codoped Ga_2O_3 branched structures has been investigated by Raman spectroscopy and XPS techniques. Figure 8 shows the peaks of the Raman spectra obtained from undoped, Sn doped, and Sn, Cr codoped nanowires. All the peaks correspond to β-Ga_2O_3.[20,21] For Sn doped structures, Raman spectra show almost no differences in the peak positions or the fwhm of the Raman peaks, in comparison with undoped Ga_2O_3, as could be expected since the tin concentration is very low. The only appreciable difference is the intensity ratio of the peaks at 651 and 657 cm^{-1} (Figure 8e). This difference was also observed in In doped β-Ga_2O_3, in which the 651 cm^{-1} peak dominated the In doped region.[21] Nevertheless, although Sn impurities influence the final morphology and shape of the microstructures, the crystalline quality of branched structures remains very high, as shown by TEM. This quality is also reflected in the vibrational spectra in these structures.

On the other hand, for Cr doped branched structures, some differences in the Raman spectra arise. In particular, a clear broadening of the peak and a higher energy shoulder are observed in the 350 cm^{-1} region (Figure 8b). The appearance of an additional component, usually at higher energy, is expected for dopant ions which have the same valence state and are lighter than the host ion,[22] which is the case of Cr^{3+} substituting Ga^{3+}. The monoclinic gallium oxide unit cell contains four Ga_2O_3 molecules. Two chemically distinguishable cationic sites are coordinated either tetrahedrally or octahedrally with oxygen ions. The crystal structure is a double chain of GaO_6 octahedra arranged parallel to the b-axis of the lattice,

dx.doi.org/10.1021/jp3093989 | J. Phys. Chem. C 2013, 117, 3036−3045

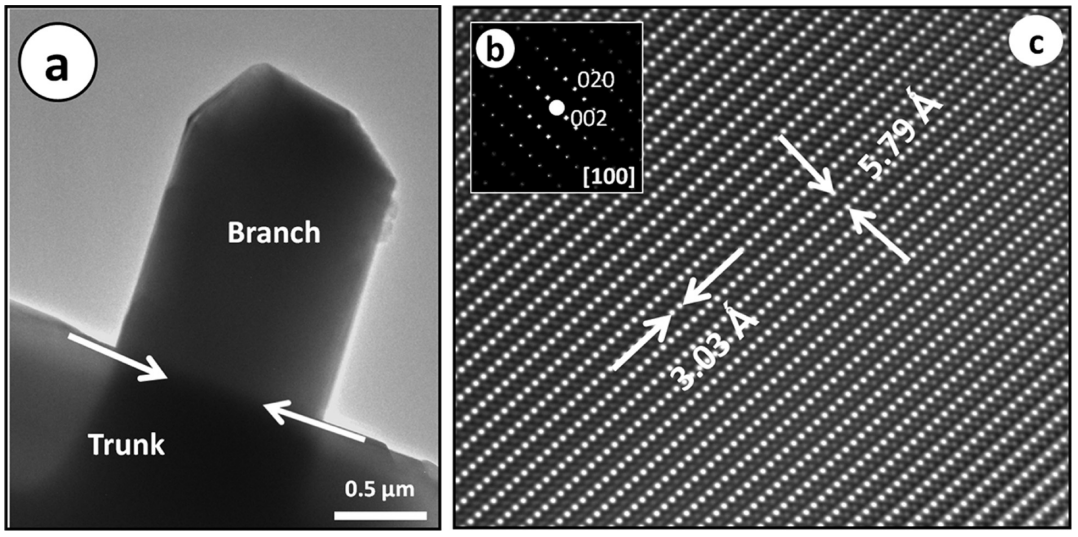

Figure 6. (a) Low magnification TEM image of a junction of a trunk and a branch in a branched structure.b SAED pattern along the [100] zone axis and (c) and the corresponding HRTEM micrograph.

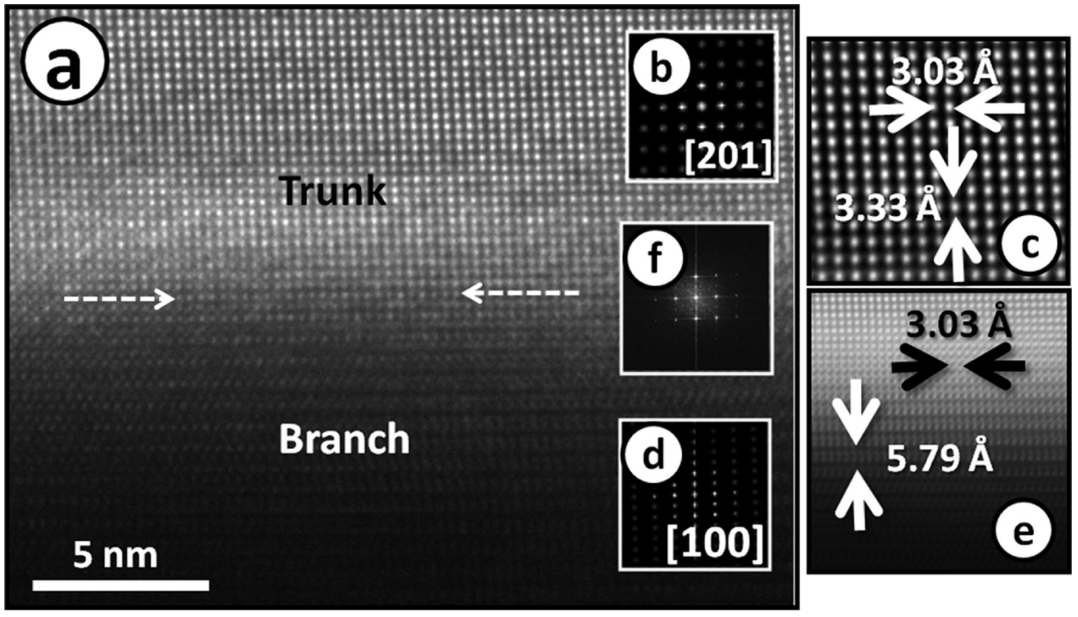

Figure 7. (a) HRTEM image of the interface region marked in Figure 6. (b) FFT pattern of the trunk along the [201] direction (c), and corresponding I-FFT. (d) FFT pattern along [100] direction of the branch and (e) corresponding I-FFT (e). At the interphase (marked by dashed arrows) the overlapping between both of the FFT patterns is seen in part f.

which is connected by GaO_4 tetrahedra. It is well-known that Cr^{3+} ions in β-Ga_2O_3:Cr^{3+} replace the Ga^{3+} ions in oxygen octahedral sites[23] and the 350 cm^{-1} Raman peak was associated to octahedron modes.[20] Therefore, the inclusion of Cr as a dopant explains the appearance of the higher energy shoulder for the 350 cm^{-1} peak. Codoping with Sn and Cr also enhances the intensity ratio variation of the 651 and 657 cm^{-1} peaks, as observed in Figure 8e. The rest of the peaks present very slight differences in positions and fwhm.

X-ray photoelectron spectroscopy (XPS) technique with spatial resolution has also been applied to investigate the local electronic features of these branched structures, and the results are summarized in Figure 9. Energy axis in high resolution XPS spectra was calibrated by fixing the C 1s binding energy (BE) at 284.8 eV.[21] Figure 9a shows an XPS map representing the intensity of the Ga 3d line of a Sn doped structure, which is representative of the samples investigated. The corresponding XPS spectra of Ga 3d and Sn 4d core levels at two different points of the wire are shown in Figure 9b. The results confirm the presence of tin in the Ga_2O_3 nanowires. High resolution XPS spectra and their deconvolution into Gaussian components of Sn 3d and O 1s core levels from this structure are shown in Figure 9c,d. The Sn $3d_{5/2}$ and Sn $3d_{3/2}$ peaks are centered at 488.2 and 497.0 eV, respectively. A value of 486.6 eV has been assigned to Sn $3d_{5/2}$ peak for Sn^{4+} in SnO_2 host.[24,25] This value is slightly lower than our measured data which is due to the fact that the actual host for Sn atoms is Ga_2O_3. On the other hand, the binding energy of O 1s core level in oxides is usually very sensitive to variations in its chemical binding. In our case, we have found that the XPS spectra of the O 1s line can be decomposed into four peaks, centered at 531.2, 531.9, 532.7, and 533.4 eV. This reveals the

dx.doi.org/10.1021/jp3093989 | J. Phys. Chem. C 2013, 117, 3036−3045

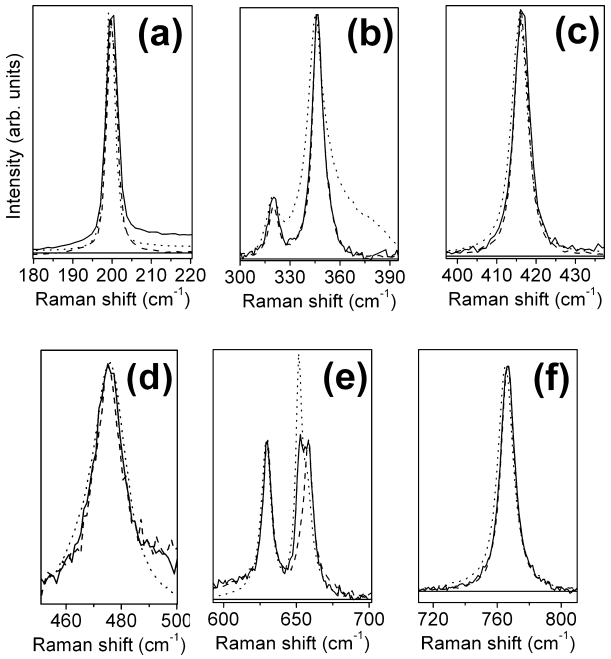

Figure 8. Comparison of the Raman peaks (normalized intensity) for undoped (---), Sn doped (—), and Cr, Sn codoped (···) nanostructures.

complexity in chemical bonds involving oxygen. In undoped Ga_2O_3, two peaks were found (531.88 and 533.45 eV) for O 1s core levels, which were assigned to Ga−O−Ga bonds and to the hydroxide (OH)/adsorbed oxygen $(O_2)^{2-}$ species, respectively.[21] They coincide with the second and the fourth components found in the Sn doped Ga_2O_3 branches. In addition, some of the oxygen atoms may be bonded to tin atoms. Values in the range 531.0−531.5 eV have been reported for the binding energy of O 1s peak in SnO_2[24,25] which enables us to assign the lower energy component at 531.2 eV peak (first component in our spectrum) to Sn−O bond. Finally, the third component at 532.7 eV could be related to some impurities in the surface. Therefore, XPS results show that Sn atoms have been effectively incorporated into the oxide matrix and participate in the chemical bonding.

After the codoping process, the XPS analysis does not reveal either Cr (e.g., Cr 3p with BE ≈ 44 eV or 3s with BE ≈ 77 eV[25]) or Sn core levels energies, indicating a very low concentration of these elements on the surface of the structures. However, differences with respect to the Sn doped sample occur. Figure 9e shows the high resolution XPS spectrum of the O 1s peak, for a Cr, Sn codoped wire, with a complex structure. Besides the binding energy components (531.3, 531.9, 532.6, and 533.5 eV) observed for Sn doped wires, two additional components seem to be necessary to fit experimental data with binding energies of 529.6 and 530.2 eV, which could be assigned to O 1s in Cr_2O_3 or in SnO.[25]

Codoping with Sn and Cr is obtained during the second thermal treatment, using the branched structures as starting material as detailed in the Experimental Section. Due to the fact that XPS is surface sensitive, these results indicate that the amount of Sn close to the surface of these samples is below the detection limit of this technique. This can be due to the fact that during the Cr diffusion process no extra tin was incorporated into the furnace. On the other hand, we have previously shown[5,16] that Cr is incorporated into the nanowires by the thermal diffusion process used in this work. This is further confirmed by the luminescence results shown below. The fact that Cr is not observed by XPS indicates that, close to the surface, the concentration is too low to be detected by this technique.

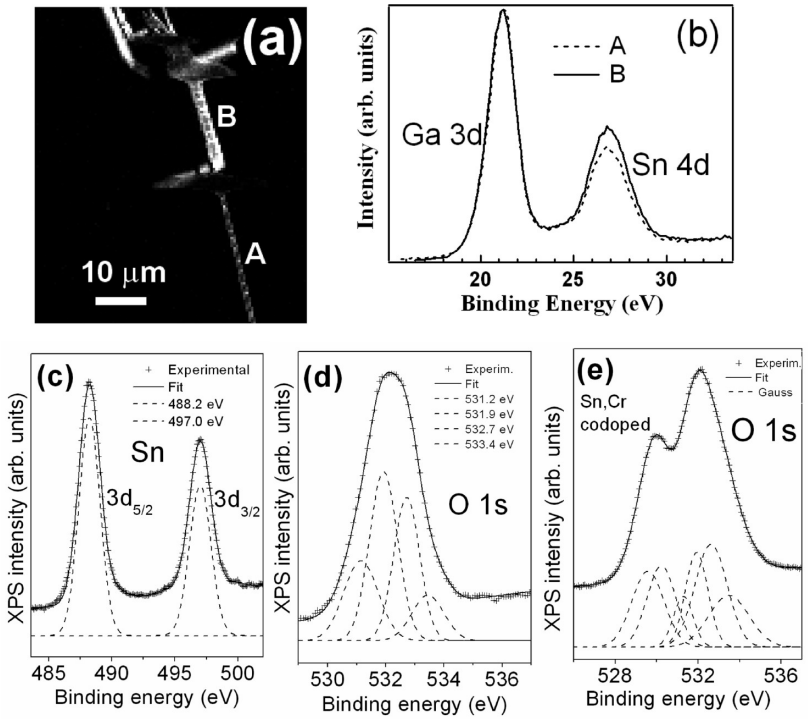

Figure 9. (a) XPS Ga 3d map. (b) Ga 3d and Sn 4d, (c) Sn 3d, and (d) O 1s spectra from a Ga_2O_3:Sn wire. (e) O 1s spectra from Ga_2O_3:Sn,Cr nanowire.

dx.doi.org/10.1021/jp3093989 | J. Phys. Chem. C 2013, 117, 3036−3045

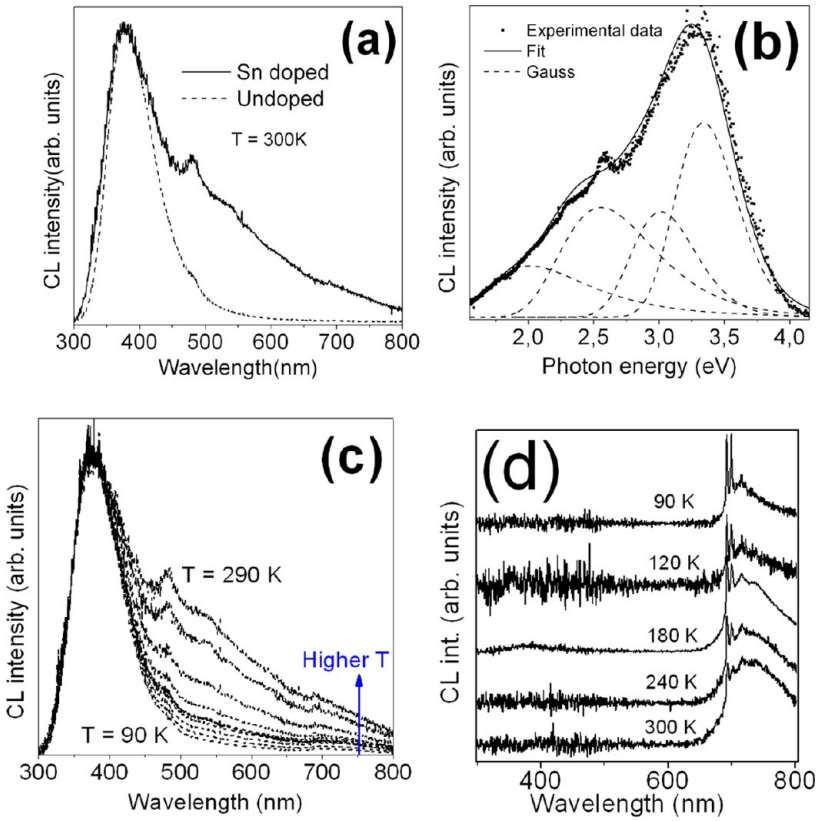

Figure 10. (a) CL spectra at RT from Sn doped sample and undoped β-Ga_2O_3 sample. (b) Detail of the composed bands in Sn doped Ga_2O_3 structures. (c) Temperature evolution of the CL emission from the Sn doped sample and (d) temperature evolution from the Sn−Cr codoped sample.

3.3. Influence of Doping on Luminescence Properties of Branched Structures. Although the main impact of Sn impurities during the growth of Ga_2O_3 nanowires seems to be connected with morphology and shape features leading to the formation of branched wires, an effective doping of these wires is also achieved during the growth process. The concentration of tin has been detected by XPS and EDS in TEM. As these structures could be used as templates for optical applications as we will show below, the characterization of their luminescence properties is worth doing. We have assessed the effect of Sn doping in the optical properties of Ga_2O_3 branched structures by cathodoluminescence (CL) in the SEM. Figure 10a plots the room temperature (RT) CL spectrum from a bunch of Sn doped nanowires. A CL spectrum from undoped nanowires is also included for comparison. In spite of the low Sn concentration in the wires, a broad band in the whole visible range is observed, in clear contrast with the undoped wires, in which a narrower characteristic β-Ga_2O_3 UV-blue emission is obtained.[26] Figure 10b shows the Gaussian deconvolution of the CL spectrum shown in Figure 10a, with three main components centered at 2.4, 3.1, and 3.4 eV. The 3.1 and 3.4 eV bands are well-known in β-Ga_2O_3 and have been assigned to intrinsic defects, such as oxygen vacancies, or some very low concentration of impurities.[7,26] The green band (2.4 eV) would be related to the presence of Sn in the wires which agrees with some previous reports. In particular, Miyata et al. obtained by electroluminescence in Sn doped Ga_2O_3 films a similar broad emission with a main peak at around 450 nm and a shoulder with its maximum in the green region,[13] which resembles the spectrum observed by CL in our experiments. Maximenko et al. have also reported a broad visible emission in Sn doped Ga_2O_3 nanowires with a main peak at around 400 nm with a shoulder in the green region,[10] which they attribute to recombination between donor levels, introduced by the incorporation of Sn atoms, and holes at the valence band in Ga_2O_3. Figure 10c shows the temperature evolution of the luminescence of Sn-doped nanowires, from 90 K to room temperature. The interesting feature observed is the quenching of the green band when the temperature decreases, so that at low temperature the CL spectrum is only composed by the characteristic bands of undoped β-Ga_2O_3 at T = 90 K. This result seems to indicate a thermally activated (phonon assisted) transition to promote carriers to the Sn-related emitting center level, or a faster increase of the intensity of the rest of the components at lower temperatures. Figure 10d shows the CL spectra of the Sn and Cr codoped sample at different temperatures. In this case, the dominant band corresponds to the red band related to Cr ions while other emissions previously observed in the Sn doped wires are completely quenched. This strong red emission is due to the characteristic Cr^{3+} R lines and phonon assisted $^4T_2 - {}^4A_2$ band.[16] The evolution with temperature is the expected one for the competition between the R lines and the broad $^4T_2-{}^4A_2$ band.[16]

These results show the high quantum efficiency of Cr ions' emission, even at room temperature, in gallium oxide hosts, which led to the quenching of the green and the violet-blue emissions which are in competition with the Cr^{3+} intraionic transition. The very high efficiency of Cr ions quenches the radiative transitions between energy levels related to native defects in Ga_2O_3.

dx.doi.org/10.1021/jp3093989 | J. Phys. Chem. C 2013, 117, 3036−3045

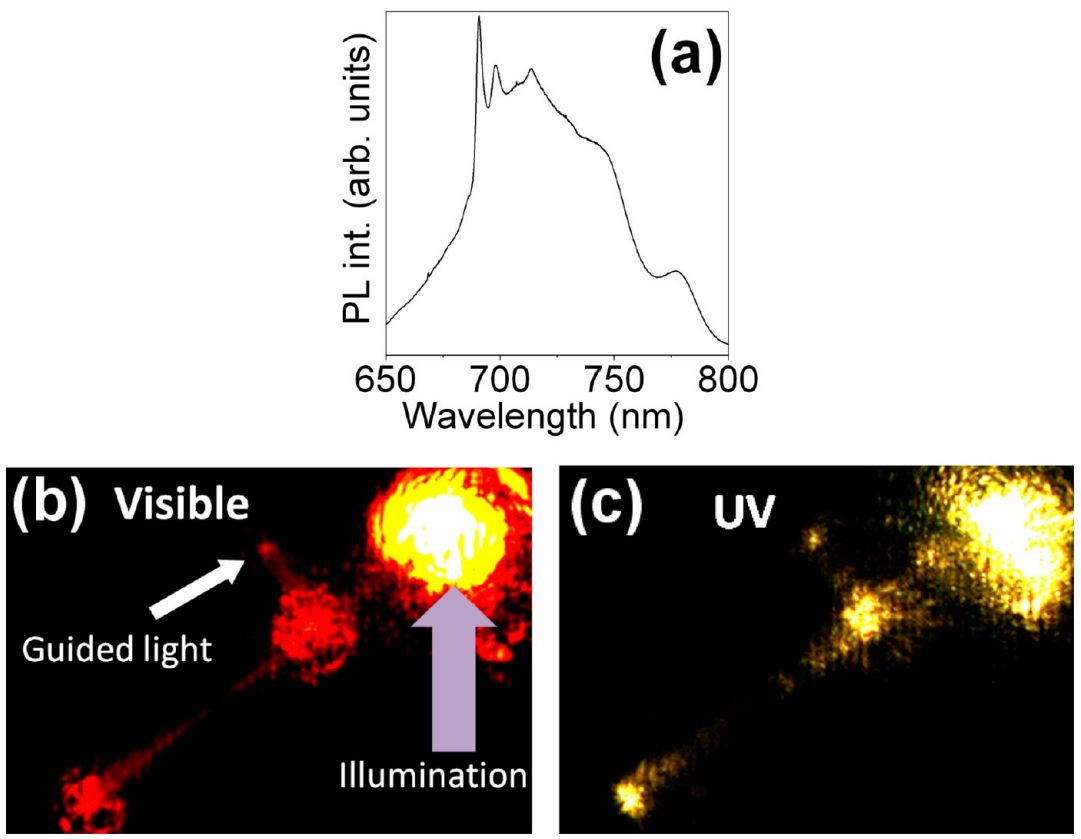

Figure 11. (a) PL spectrum from the branched wire shown in Figure 5b. (b) Room temperature μ-PL with a 325 nm HeCd laser line excitation of the same branched structure. (c) UV radiation bright field image.

We have used the codoped samples to study the propagation that the red light generated by Cr ions follows through these branched structures. Figure 11a shows the micro-PL spectrum from the Sn, Cr codoped wire shown in Figure 5b. In this case, the 325 nm (3.82 eV) HeCd laser line of the confocal microscope produces below band gap excitation, and strong red emission due to the Cr^{3+} intraionic transitions is observed. Excitation of the Cr^{3+} is indeed obtained through the excitation band centered at around 3.9 eV present for this ion in β-Ga_2O_3.[16] Figure 11b shows the corresponding visible μ-PL image of the wire. Under illumination with the laser at the upper end of the wire (violet arrow), the intense luminescence created is guided along the trunk and also transmitted through the perpendicular branch, as is clearly seen in the bright red spot highlighted with a white arrow in Figure 11b. UV laser radiation is also guided along the trunk and branch, as seen in Figure 11c for the 325 nm line of the laser.

As shown in the CL spectra, the luminescence of β-Ga_2O_3 nanowires covers the whole visible range, and the emission wavelength can be adjusted by properly selecting the kind and concentration of dopants. In fact, doping of these branched structures with other optically active ions in order to obtain luminescence from the UV to the IR is possible by other doping methods such as ion implantation.[27] Besides, the branched morphology can be very useful for some specific applications such as photonic routers and beam splitters.[19,28,29] Besides, resonant modes have been found within these structures.[30]

CONCLUSIONS

Elongated Sn doped gallium oxide structures have been obtained through a thermal evaporation method. The presence of Sn leads to the formation of branches. In a further thermal step, the branched structures have been codoped also with Cr. The crystal quality has been found to be very high by TEM–HRTEM analysis, and the mechanisms for the formation of the branches have been discussed, finding epitaxial growth as one of them. The presence of Sn and Cr within these structures does not strongly influence the vibrational properties, as analyzed by Raman microspectroscopy. Luminescence in the whole visible range is obtained by codoping with Sn and Cr. For the first dopant, a broad emission covering most of the visible range is observed by CL, with strong peaks in the UV-blue and green ranges. When codoping with chromium, the luminescence is virtually composed exclusively by the intense red band characteristic of Cr^{3+} in this oxide. Branched, Sn, Cr codoped structures behave as efficient waveguides along their trunks and branches, both for the UV and visible light, as observed with microphotoluminescence imaging.

AUTHOR INFORMATION

Corresponding Author

*E-mail: emilio.nogales@fis.ucm.es.

Notes

The authors declare no competing financial interest.

ACKNOWLEDGMENTS

This work has been supported by MICINN through Projects MAT 2009-07882 and Consolider Ingenio CSD 2009-00013.

The authors are grateful to Dr. Luca Gregoratti at the Sincrotrone Elettra Trieste for useful advice on XPS measurements.

REFERENCES

(1) Barth, S.; Hernandez-Ramirez, F.; Holmes, J. D.; Romano-Rodriguez, A. *Prog. Mater. Sci.* **2010**, *55*, 563−627.
(2) Lu, J. G.; Chang, P.; Fan, Z. *Mater. Sci. Eng., R* **2006**, *52*, 49−91.
(3) Feng, P.; Zhang, J. Y.; Li, Q. H.; Wang, T. H. *Appl. Phys. Lett.* **2006**, *88*, 153107-1−153107-3.
(4) Vanithakumari, S. C.; Nanda, K. K. *Adv. Mater.* **2009**, *21*, 1−4.
(5) Nogales, E.; Garcia, J. A.; Mendez, B.; Piqueras, J. *Appl. Phys. Lett.* **2007**, *91*, 133108-1−133108-3.
(6) Nogales, E.; Mendez, B.; Piqueras, J. *Ultramicroscopy* **2011**, *111*, 1037−1042.
(7) Shimamura, K.; Víllora, E. G.; Ujiie, T.; Aoki, K. *Appl. Phys. Lett.* **2008**, *92*, 201914-1−201914-3.
(8) Varley, J. B.; Weber, J. R.; Janotti, A.; Van de Walle, C. G. *Appl. Phys. Lett.* **2010**, *97*, 142106-1−142106-3.
(9) Ronning, C.; Borschel, C.; Geburt, S.; Niepelt, R. *Mater. Sci. Eng., R* **2010**, *70*, 30−43.
(10) Maximenko, S. I.; Mazeina, L.; Picard, Y. N.; Freitas, J. A.; Bermudez, V. M.; Prokes, S. M. *Nano Lett.* **2009**, *9*, 3245−3251.
(11) Higashiwaki, M.; Sasaki, K.; Kuramata, A.; Masui, T.; Yamakoshi, S. *Appl. Phys. Lett.* **2012**, *100*, 013504−1−013504−3.
(12) Lopez, I.; Nogales, E.; Hidalgo, P.; Mendez, B.; Piqueras, J. *Phys. Status Solidi A* **2012**, *209*, 113−117.
(13) Miyata, T.; Nakatani, T.; Minami, T. *J. Lumin.* **2000**, *87−89*, 1183−1185.
(14) Nogales, E.; Mendez, B.; Piqueras, J.; Garcıa, J. A. *Nanotechnology* **2009**, *20*, 115201-1−115201-5.
(15) Wang, J.; Zhuang, H.; Zhang, X.; Zhang, S.; Li, J. *Vacuum* **2011**, *85*, 802−805.
(16) Nogales, E.; Garcia, J. A.; Mendez, B.; Piqueras, J. *J. Appl. Phys.* **2007**, *101*, 033517-1−033517-4.
(17) Hidalgo, P.; Mendez, B.; Piqueras, J. *Nanotechnology* **2008**, *19*, 455705−1−455705−5.
(18) Diaz, J.; Lopez, I.; Nogales, E.; Mendez, B.; Piqueras, J. *J. Nanopart. Res.* **2011**, *13*, 1833−1839.
(19) Zheng, J. Y.; Yan, Y.; Wang, X.; Zhao, Y. S.; Huang, J.; Yao, J. *J. Am. Chem. Soc.* **2012**, *134*, 2880−2883.
(20) Dohy, D.; Lucazeau, G.; Revcolevschi, A. *J. Solid State Chem.* **1982**, *45*, 180−192.
(21) López, I.; Utrilla, A. D.; Nogales, E.; Mendez, B.; Piqueras, J.; Peche, A.; Ramirez-Castellanos, J.; Gonzalez-Calbet, J. M. *J. Phys. Chem. C* **2012**, *116*, 3935−3943.
(22) *Raman Scattering in Materials Science*; Weber, W. H., Merlin, R., Eds.; Springer: New York, 2010.
(23) Yeom, T. H.; Kim, I. G.; Lee, S. H.; Choh, S. H.; Yu, Y. M. *J. Appl. Phys.* **2003**, *93*, 3315−3319.
(24) Kwoka, M.; Ottaviano, L.; Passacantando, M.; Santucci, S.; Czempik, G.; Szuber, J. *Thin Solid Films* **2005**, *490*, 36−42.
(25) http://srdata.nist.gov/xps
(26) Binet, L.; Gourier, D. *J. Phys. Chem. Solids* **1998**, *59*, 1241−1249.
(27) Nogales, E.; Hidalgo, P.; Lorenz, K.; Mendez, B.; Piqueras, J.; Alves, E. *Nanotechnology* **2011**, *22*, 285706-1−285706-7.
(28) Mieszawska, A. J.; Jalilian, R.; Sumanasekera, G. U.; Zamborini, F. P. *Small* **2007**, *3*, 722−756.
(29) Kurt, H.; Giden, I. H.; Citrin, D. S. *Opt. Express* **2011**, *19*, 26827−26838.
(30) López, I.; Nogales, E.; Mendez, B.; Piqueras, J. *Appl. Phys. Lett.* **2012**, *100*, 261910−1−261910−3.